Carbon 246 (2026) 120890

Contents lists available at ScienceDirect

Carbon

journal homepage: www.elsevier.com/locate/carbon

Observation and manipulation of grain boundary corrugations in polycrystalline graphene supported by van der Waals and metallic substrates

Xueyan Li [1], Jiaqi Yang [1], Yuang Li, Yi Pan [*]

Center for Spintronics and Quantum Systems, State Key Laboratory for Mechanical Behavior of Materials, Xi'an Jiaotong University, Xi'an, 710049, China

ARTICLE INFO

Keywords:
Polycrystalline graphene
Grain boundary
Wrinkles
Asymmetric strain
Bubble-like corrugation
Polarity switching

ABSTRACT

The nanoscale corrugations, which endow atomically thin two-dimensional materials with unique physical and chemical properties, universally exist in the grain boundary (GB) of polycrystalline graphene, but their structural tunability and the influence of substrate interaction require further investigation. Here, we report the atomically resolved scanning tunneling microscope (STM) observation and manipulation of GB corrugations in polycrystalline graphene with different substrate interactions. On the van der Waals (vdW) substrate graphite, the structure of the GB corrugation is dominated by intralayer interaction arising from the misorientation between neighboring grains. It evolves from periodic bubble-like corrugations to continuous wrinkles as the misorientation angle increases. The buckling polarity of the surface and subsurface bubble-like GB corrugations on vdW substrates can be reversibly manipulated by applying an electric field through the STM tip. While on the metallic substrate Pt(111), the GB wrinkles show asymmetric cross-sectional profiles due to combined intralayer interactions from neighboring grains and interlayer interactions from the substrate. The metallic substrate also provides the pinning effect prohibiting the buckling polarity manipulation. Additionally, an asymmetric strain distribution mechanism was proposed to explain the influence of the key factors. These findings shed light on the strain engineering of graphene corrugations, which might find applications in electronic devices.

1. Introduction

The surface corrugations, like wrinkles, ripples, and bubbles, are commonly existing in atomically thin two-dimensional (2D) materials supported by various substrates. Although they are usually considered as structural imperfections that need to be eliminated, recent studies reveal that the corrugations would bring about some unique physical and chemical properties [1–5]. In particular, the physical properties like local magnetic, electronic, optoelectronic, and flexoelectric characteristics could arise from such structural corrugations. For example, large pseudo-magnetic fields in natural or fabricated graphene nanobubbles [1,6], single photon emitter in locally strained nano-spots in monolayers transition metal dichalcogenides (TMDC) [4,7], carrier mobility tuned by wrinkles in graphene [8] and MoS_2 [3], nanoscale wrinkles facilitated proton transport in h-BN and graphene [2], as well as the enhanced polarity in wrinkled ferroelectric thin film of $CuInP_2S_6$ [5]. Moreover, the chemical properties of 2D materials could also be significantly influenced by the wrinkles, allowing for precise modulation of chemical reactivity through wrinkle engineering [9]. Thus, the corrugations are increasingly drawing research interest for their potential in device applications, e.g., ultra-thin memory devices based on the carrier trapping in wrinkled 2D monolayer MoS_2 [10] and strain sensors that utilize modulated wrinkles on flexible substrates [11].

The physical origin of the surface corrugations in graphene is mainly the relaxation of local strain, which was introduced into the lattice either during growth or after growth. During the growth process, strain is often induced by thermal expansion coefficient mismatch [12–14], lattice mismatch with lateral heterostructure [15], and the substrate morphology [16–18]. In contrast, there are more factors to induce strain during the post-growth treatments, including the inhomogeneous breakage of layered vdW forces [19,20], elastic modulus mismatch [21], and the corrugated substrate for transfer [22]. In the case of elastic modulus mismatch, prior studies demonstrated that pre-strained elastomer substrated could facilitate controllable fabrication of periodically

* Corresponding author.
E-mail address: yi.pan@xjtu.edu.cn (Y. Pan).
[1] Contributed equally.

https://doi.org/10.1016/j.carbon.2025.120890
Received 8 August 2025; Received in revised form 21 September 2025; Accepted 25 September 2025
Available online 25 September 2025

wrinkled graphene [23]. Conprehensive Raman investigation further reveals the efficient interfacial stress transfer from the pre-strained soft polymer substrate [21]. Interestingly, the GBs in polycrystalline graphene inherently exhibit strain that needs to be relieved due to grain misorientation. Moreover, the strain distributions across different GBs are also influenced by interactions between graphene and the substrates. A theoretical study has predicted that the energy balance between intralayer chemical and interlayer mechanical energies would drive the deformation that extends in the third dimension, forming various corrugations in the GBs [24]. Some peculiar phonon excitation characteristics of wrinkles and blisters of graphene on metal substrates have been revealed in the electron tunneling spectroscopy [25,26]. However, atomic-scale observation and manipulation of graphene GB corrugations on different types of substrates, which are crucial for the formation mechanism of corrugated GBs, are still lacking.

In this work, we investigated the GB corrugations in polycrystalline graphene on vdW and metallic substrates based on *in situ* STM measurements in ultra-high vacuum (UHV) environment. We chose the highly oriented pyrolytic graphite (HOPG) and silicon carbide (SiC) with epitaxial graphene as vdW substrates, while the single crystal platinum (Pt) as metallic substrates. The polycrystalline graphene samples, consisting of grains with misorientation angles ranging from 0° to 30°, were prepared to systematically demonstrate the structural evolution of the GB corrugations, i.e., out-of-plane buckling in various forms including wrinkles and bubbles. STM tip manipulation has been employed to realize the reversible switching of single GB bubbles buckling polarity by applying an electric field through the tip. Furthermore, a comparative study was conducted to analyze the contributions of intralayer and interlayer interactions and their combined impact on GB morphology. To further investigate strain distributions across different GBs, cross-sectional profile analysis of STM topographic images was performed, showing height variations and asymmetry of corrugations. Based on these results, a local strain distribution mechanism was proposed to explain the influence of the key factors. These findings provided in-depth insights into the formation mechanism and local strain engineering of GB corrugations in polycrystalline graphene.

2. Experimental section

2.1. Polycrystalline graphene sample preparation

Polycrystalline graphene with GB wrinkles has been prepared on two types of substrate: the vdW substrates with weak interfacial interaction and the metallic substrates with relatively stronger interfacial interaction. The first vdW substrate is a commercially available (Institute of Metal Research, CAS) class II HOPG with an average grain size of 10^2 nm, which was mechanically cleaved with scotch tape in air and degassed at 473 K for 2 h in a UHV chamber before STM measurement. The second vdW substate is a *C*-Face SiC$(000\bar{1})$ crystal (TanKeBlue), which was degassed at 1500 °C in a H_2/Ar mixture (molecular weight ratio 1:4, 500 Torr) for 30 min. The polycrystalline multilayer graphene was grown on SiC$(000\bar{1})$ by annealing at 1500 °C in a 100 % Ar atmosphere (700 Torr) for 15 min. The samples were degassed at 550 K in UHV before STM measurement. The metallic substrate we chose is Pt (111) single crystal (MaTeck GmbH), which has been prepared with surface orientation accuracy $< 0.5°$, and one-sided polishing with surface roughness <10 nm. It was cleaned by performing cycles of Ar ion sputtering followed by annealing to 1200 K till no signals of contaminants were observable in the Auger Electron Spectroscopy (AES) spectrum. The polycrystalline graphene was grown by exposing the hot Pt (111) substrate to high-purity (99.995 %) ethylene, then ramping the temperature down to room temperature in a short period of 5 min. The graphene growth procedures on SiC and Pt substrates followed established methods detailed in Refs. [27–29].

2.2. STM characterization and GB bubble manipulation

The experiments were carried out in a UHV chamber with the base pressure lower than 1×10^{-10} mbar. The chamber is equipped with an STM, an AES, and a LEED. The STM measurements were performed in a liquid Helium cooled cryogenic STM (CreaTec) operated at ~ 4.7 K. We use homemade electrochemically etched tungsten tips, which were cleaned by Ar ion sputtering and tested on Au(111). The topographic images were taken in a constant-current scanning mode. The bias voltages refer to the sample with respect to the tip. The details of angle measurement, height measurement, and uncertainty margins are presented in Note 1 of the Supporting Information.

The bubble-like GB corrugations were flipped by placing the tip at the top (from up-to downward) or off-center top position (from down-to upward) of the target bubble, then maintaining a small tip-sample distance (Bias $V_b = \pm 0.01$ V, tunneling current $I_t = 2$ nA) for 5–10 s. To avoid unintentional flipping, the topographic images were taken at a larger tip-sample distance ($|V_b| > 0.5$ V, $I_t < 0.5$ nA).

3. Results and discussion

3.1. GB bubbles and wrinkles on vdW substrates

Firstly, we investigated the GB morphology of polycrystalline graphene on HOPG by measuring the atomic structure and height profile of the GB between misoriented grains. Depending on the misorientation angles (θ), as displayed in the STM images in Fig. 1(a–c), the GB shows two distinct corrugations, namely the GB bubbles and the GB wrinkles. As shown in Fig. 1(a), the atomic resolution STM image taken at the GB with a small misorientation angle reveals typical bubble-like out-of-plane corrugation (the overview images are presented in Fig. S1), corresponding to the structure model in Fig. 1(g). The Fast Fourier Transform (FFT) pattern obtained from atomic resolution STM images presents two sets of hexagonal lattices with a rotational angle of $\theta = 5.8°$, which is the exact misorientation angle between the neighboring grains. Fig. 1(a) also reveals that the GB bubbles are periodic, while the bubble along the GB forms a one-dimensional (1D) chain with a periodicity of 2.4 nm. The schematic structure model in Fig. 1(g) further reveals that the out-of-plane buckling is induced by strain relaxation around the 5–7 carbon atom ring pairs connecting the two grains rotated 2.9° with each other. Fig. 1(d) shows the height profile along the green dashed line in Fig. 1(a), indicating that the height of the bubble is about 0.5 nm. Such bubble-like structures were also observed at the GB of epitaxial multilayer polycrystalline graphene on SiC $(000\bar{1})$, as shown in Fig. S2. It is evident that on vdW substrates, small misorientation angles typically induce the formation of GB bubbles.

When the misorientation angle increases, the bubble chain will gradually merge together and form a continuous wrinkle. As shown in Fig. 1(b) and (e), the GB wrinkle with a height of 0.07 nm has been formed between two grains with a misorientation angle of $\theta = 21.4°$. In other words, the two grains rotated 10.7° in opposite directions, as schematically indicated in Fig. 1(h). The 5–7 carbon ring pairs are much denser at the GB. Thus, the periodicity will continue to decrease as the misorientation angle increases. As an example, we show that a more flattened wrinkle appears at the GB with a misorientation angle of $\theta = 26.8°$, as shown in Fig. S3 and S4. Obviously, when the misorientation angle exceeds a critical threshold, the GBs will stably adopt wrinkles.

Interestingly, we also observe a special low GB wrinkle appears between two grains with the same orientation, as shown in Fig. 1(c). High-resolution STM image reveals that there is a dislocation line due to the non-perfect spacing when the neighboring grains merge together, as indicated in Fig. 1(c). Such a dislocation line is composed of 1D defects, manifested as periodically repeating non-hexagonal rings along the GB, as schematically indicated in Fig. 1(i) lower panel. The strain on the dislocation line only causes a minor wrinkle, in stark contrast to the

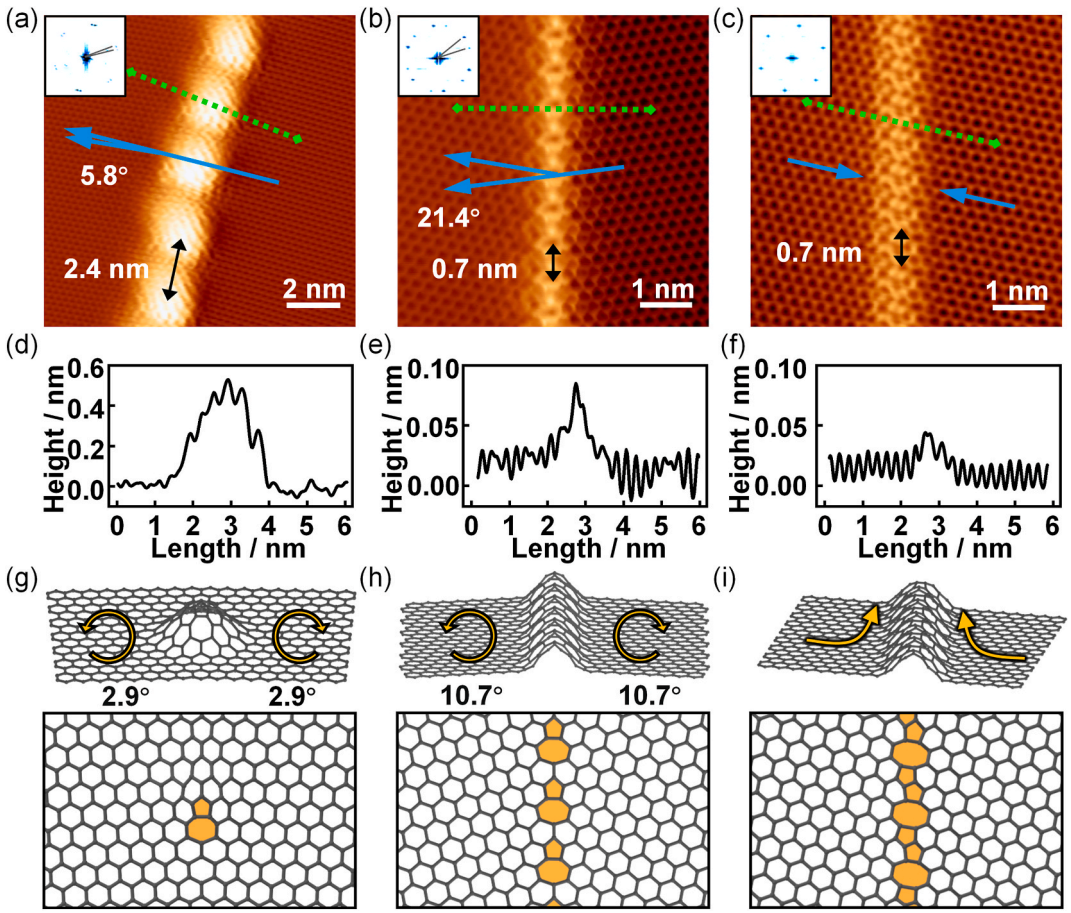

Fig. 1. GB corrugations on HOPG. (a–c) Atomic resolution STM images of three different GB corrugations on HOPG. The insets in panels (a–c) display the corresponding FFT images. (a: $V_b = -0.7$ V, $I_t = 0.32$ nA, b: $V_b = -1$ V, $I_t = 0.32$ nA, c: $V_b = -0.8$ V, $I_t = 1$ nA). The zigzag directions of graphene lattices are indicated by the blue arrows. Angular error $\leq 0.6°$. (d–f) The height measurement along the green dashed arrows in (a–c). (g–i) The schematics of three different GB corrugations correspond to (a–c). (g–h) The GBs are formed between two adjacent grains with misorientation angles of 5.8° and 21.4°. (i) The GB is formed by translating two adjacent grains to each other along the direction of the vertical GB wrinkle. The orange arrows show clockwise (counterclockwise) rotation and slip of the graphene layer with respect to the underlying graphene, respectively. (For interpretation of the references to colour in this figure legend, the reader is referred to the Web version of this article.)

significant wrinkling caused by misorientation angle formation, as shown in Fig. 1(f). While the measured heights exhibit slight voltage-dependent variations, these minor discrepancies do not affect our overall conclusions, as shown in Fig. S5.

These results confirmed that the out-of-plane corrugation is a universal structural feature in the GB of polycrystalline graphene on vdW substrates. The shape and height of the corrugation are highly dependent on the misorientation angle ($0° < \theta < 30°$) between the neighboring grains. When two misoriented graphene islands meet each other and merge together, edge-sharing hexagonal and non-hexagonal rings are formed at the GB, normally with slightly higher density of carbon atoms due to the abundant supply of carbon precursors during growth. Such non-perfect sp^2 hybridization bonds would introduce compression strain into the lattice. The out-of-plane deformation could efficiently release the compression strain by adjusting the bond angle, requiring only minimal deformation to significantly reduce the GB energy. In contrast, in-plane deformation requires significant compression of *C*–C bonds, which would lift the GB energy in our case. Such a strain relaxation requires the carbon atom to shift into the third dimension, naturally out of plane upwards, which is the origin of the GB corrugations. In some special cases, like a perfect GB loop [30], the GB remains flat due to high bending rigidity [31]. Additionally, increasing the misorientation angle would tune the strain distribution in the form of wrinkles or bubbles in varying periodicity. It is noteworthy that the optimized misorientation angles in theoretical or simulation models are normally deduced by minimizing the system energy, while in real materials with a substrate, the angle has been determined by the orientations of the two neighboring grains at their nucleation stage (Fig. S6). Nonetheless, the trend we observed is in nice agreement with the earlier theoretical study by J. Carlsson et al. [32] and molecular dynamic simulations by Tong et al. [33] with the absence of substrate interaction. Generally, the shape of the GB corrugation is dominated by the misorientation angle, while the substrate plays an insignificant secondary role.

Most previous works do not take the contribution of the vdW substrate into account since the interaction is very small [34–38]. However, we notice that the substrate would still break the symmetry between the two neighboring grains. Even on vdW substrates, the stacking order and layer rotational angle would be different for the two grains. Thus, the asymmetric strain distribution is a universal character in the GB. Consideration is given to two distinct orientations, i.e., across and along the GB. In the direction along the GB, the highly local asymmetric strain at the bubble is gradually reduced along the GB since the non-hexagonal carbon rings become denser with increasing misorientation angles. In the direction across the GB, the line profile curves reveal that the height and asymmetry of the GB corrugation are both gradually decreasing with increasing misorientation angles, indicating the local strain asymmetry is decreasing as well. The observation of a low-amplitude wrinkle along the dislocation line suggests a symmetrically distributed, minimal strain across the GB.

3.2. Tip manipulation of GB bubbles

Compared with the case of the free-standing graphene, the vertical geometric symmetry of graphene supported by the substrate is broken due to interfacial interaction. As a result, the initial structure of the experimentally observed GB bubbles is always buckled upwards, as shown in Fig. S7, although theoretical calculations predict an equivalent probability of up- and down-wards buckling [39]. Here, we show that the buckling polarity, i.e., upward or downward, could be manipulated by using the STM tip. Specifically, the GB bubbles could dynamically flip between upward and downward buckling, since they are a bi-stable structure with a relatively low energy barrier. Fig. 2(a) shows a GB bubble chain on vdW substrates between two grains with misorientation angles of $\theta = 12.2°$. Taking the pinned defect (marked by a black circle) as a reference, five bubbles on the right are all buckling upward at the initial stage. When the local electric field is applied to the upward-buckling bubbles indicated by the black arrows in Fig. 2(a), they are flipped into the downward-buckling state as shown in Fig. 2(b). The polarity manipulation was realized by moving the tip at the center of bubbles and maintaining for about 5–10 s, as schematically demonstrated in Fig. 2(d). By repeating the manipulation on the fourth bubble, it was flipped as well, as shown in Fig. 2(c). The tip-assisted manipulation is reversible, as shown in Fig. S8. Flipping from downward to upward can be achieved by making the manipulation maneuver at a

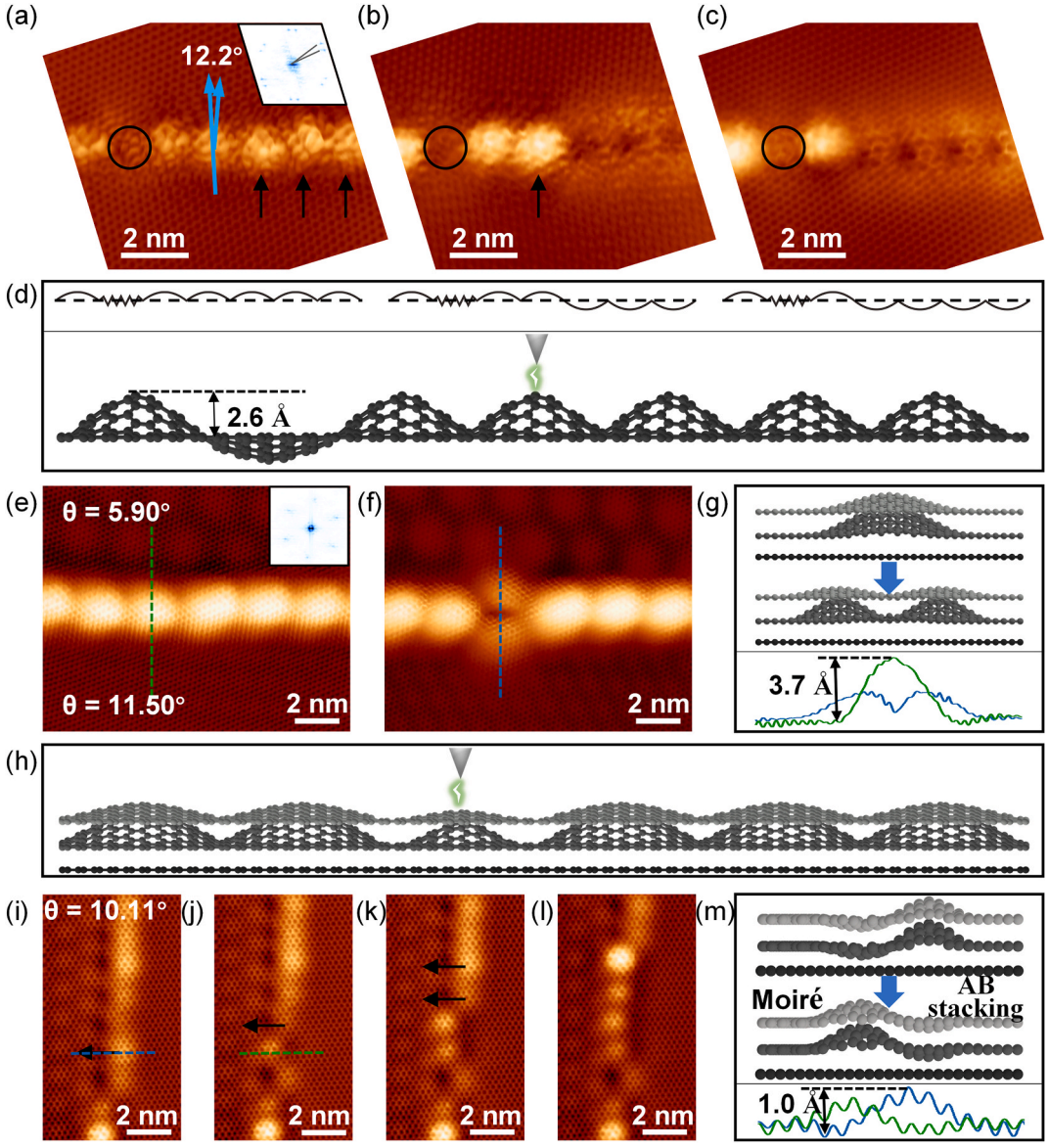

Fig. 2. (a–c) STM images of GB bubbles with a misorientation angle of 12.2° on HOPG reveal a dynamic flip between upward and downward buckling, with the zigzag directions of the graphene lattices marked by blue arrows (a–c: $V_b = -0.7$ V, $I_t = 0.32$ nA). The inset in (a) displays the FFT image. Black arrows highlight bulges flipped by the STM tip under an electric field. A pinned defect is marked by a black circle. Angular error: ±0.5°. (d) Upper panel: Schematic representation of the bubble-like structure corresponding to (a–c). Lower panel: Zoomed-in schematic illustrating the bubble-like structure in (a) and the manipulation of the bubble by the tip. (e–f) STM images of subsurface GB bubbles on HOPG (while the top layer graphene remains intact) show a dynamic flip between upward and downward buckling (e–f: $V_b = -0.7$ V, $I_t = 0.32$ nA). The inset in (e) displays the FFT image. Angular error ≤ 0.07°. (g) Upper panel: Side view of a single bubble illustrating the process of defect flip from (e) to (f). Lower panel: Corresponding bubble profiles along the green and blue lines in (e–f). (h) Zoomed-in schematic illustrating the bubble-like structure in (f) and the manipulation of the bubble by the tip. (i–l) STM images of the gradual evolution of the subsurface GB wrinkle on the right side to a GB bubble chain on the left side (i–l: $V_b = -1$ V, $I_t = 0.32$ nA). Black arrows highlight bulges flipped by the STM tip under an electric field. Angular error: ±0.12°. (m) Upper panel: Side view illustrating the process of a single bubble shift from right to left. Lower panel: Corresponding bubble profiles along the blue and green lines in (i–j). (For interpretation of the references to colour in this figure legend, the reader is referred to the Web version of this article.)

slightly off-center position of the bubbles. Fig. 2(d) schematically illustrates the polarity manipulation process, where the upper panels represent the cross-sectional profile of Fig. 2(a–c), respectively. These results confirmed that the GB bubbles could be effectively manipulated by applying a local electrical field that triggers the switching of the bi-stable structure between two states, since the inelastic electron scattering energy injected by the STM tip exceeds the strain energy induced barrier. The mechanism of the tip manipulation might be contributed by various effects, including dipole interaction originating from the flexoelectricity of the bubble [31,40], electrostatic interaction from tip-induced image charge, and the vdW interactions [41–43]. Our experiments suggest the vdW interactions are playing a dominant role, as explained in Note 2 of the supporting information. We also noticed that the upward-buckling state is slightly favored over the downward state, most likely due to the limited interfacial space between the film and the substrate, which broke the vertical symmetry of the GB bubbles.

Additionally, we have found that the polarity of GB bubbles could be manipulated even when they were buried underneath a complete sheet of graphene, which also appeared as top layer corrugation due to the strain induced by the GB bubbles below. Fig. 2(e) shows a bubble chain (the overview images are presented in Fig. S10) that looks like the surface GB bubbles, but actually, there is no GB or defects, as seen in the atomic resolution images or in the FFT pattern. However, the two sides of the bubble chain show different moiré patterns arising from an interlayer twisting. Therefore, we can attribute it to a subsurface GB with a small misorientation angle. By analyzing the moiré periodicities and orientations, it can be determined that the specific misorientation angle is 5.60°. By applying the same manipulation to the upward bilayer bubbles as demonstrated in Fig. 2(h), we successfully achieved the polarity flipping into the downward state, as shown in Fig. 2(f). The STM image also reveals that the downward corrugation shows a two-lobed shape across the GB. We conduct height profile measurements along the green (upward) and blue (downward) dashed lines in Fig. 2(e and f), respectively. It reveals that the upward bubble has flipped into two smaller upward bubbles with a concave shape in the middle, rather than the completely downward buckling as the surface GB bubbles. We attribute it to the increased in the vertical direction, since the restricted inner layer space does not allow the buckling into the bulk, giving rise to a further inequivalent strain relaxation.

Surprisingly, we found that the subsurface GB corrugations can also be shifted between two adjacent locations while maintaining the upward buckling state. It occurs when only one of the grains shows a moiré pattern. The sequence of images in Fig. 2(i–l) clearly presents the gradual evolution of the subsurface GB wrinkle on the right side to a GB bubble chain on the left side, which was achieved by tip manipulation ($V_b = 0.02$ V, $I_t = 2$ nA) at the spots marked by the arrows. The height profiles (Fig. 2(m) lower panel) taken along the lines in Fig. 2(i, j) across the GB confirmed the shifting of the corrugations, as schematically demonstrated in Fig. 2(m) upper panel. Such behavior of the subsurface GB corrugation is attributed to the two distinct stacking structures of the neighboring grains, i.e., misorientation-induced moiré pattern on one side and AB stacking on the other. Such manipulation is reversible as well, i.e., applying an electric field to the bubble on the left can shift back to the right. When the corrugation is shifted to the AB stacking grain, it appears as a wrinkle. When it is shifted to the moiré grain, it appears as a bubble chain. That is because the two sides have distinct misorientation angles with respect to the surface layer of graphene. We note that such shifting manipulation is obviously easier than the up-down manipulation, indicating a much lower energy barrier between the bistable states. Our tip-assisted manipulation of GB corrugations is highly controllable and reversible, which provides a new strategy for local strain engineering in polycrystalline graphene.

3.3. Grain boundary wrinkles on metal substrates

The metallic substrate, on the other hand, provides a non-negligible strong interfacial interaction to the polycrystalline graphene. The GB corrugation is influenced by both factors from the interlayer GB strain distribution and the intralayer interaction. The latter factor is related to the crystal orientation deviation of the grain with respect to the substrate (twist angle φ) and lattice mismatch induced moiré superstructure. To investigate the complex GB structure, we prepared multi-grain monolayer graphene on a Pt (111) substrate in a UHV chamber.

Three types of ordered GB wrinkles are observed, as shown in Fig. 3 (a)–(c). The yellow and blue arrows in each panel indicate the direction of Pt (111) and the direction of graphene grains, respectively. The orientation of graphene grains can be easily found from atomic resolution images, while the orientation of the Pt substrate is obtained from the LEED pattern. The twist angles φ of each grain with respect to the Pt substrate are easily measured and shown beside the arrows. Fig. 3(a) shows the GB wrinkle between two grains with $\varphi_1 = 29.8°$ and $\varphi_2 = 14.2°$ (the overview images are presented in Fig. S11), respectively. The wrinkle is in an irregular line, with a height of 1.2 nm and a width of 1 nm, indicated by the cross-section profile plotted in Fig. 3(d). The height profile also reveals the winkle is asymmetric across the GB, where the slope is steeper on the $\varphi_2 = 14.2°$ grain, indicating a highly asymmetric local strain distribution. Fig. 3(b) shows a GB wrinkle between two grains with $\varphi_1 = 19.2°$ and $\varphi_2 = 14.2°$, respectively. The height of the wrinkle is 0.6 nm, as is shown in the profile curve in Fig. 3(e). The cross-sectional shape is less asymmetric, as the twist angles φ difference decrease. Besides the GB of misorientation grains, anti-phase GB can be formed between the grains with the same rotational angle but opposite direction, for example, the GB between two $\varphi = 5.8°$ grains in Fig. 3(c). The anti-phase GB is very flat with almost the same height as the graphene film, indicating a less strained GB structure.

These STM observations confirm that GB corrugation is dependent on both the interaction between the neighboring grains and their interactions with the Pt (111) substrate. The height of GB on Pt (111) substrate varies with the angular difference $\varphi_1 - \varphi_2$ between the neighboring grains, as shown in Fig. 3(g). In the extreme case when a relatively flat grain meets a highly corrugated grain with moiré pattern, the GB strain will be relaxed in the way that the flat grain side will bend up while the moiré pattern side is pinned on the surface, since the stress has been released at the side that has the relatively weaker interaction with the substrate, as shown in Fig. 3(h). Consequently, the high wrinkle with asymmetric shape is formed. On the other hand, when the twist angle of the neighboring grains is similar, the GB wrinkle is much lower, as schematically demonstrated in Fig. 3(i). Without doubt, some 5-7-rings of carbon atoms will coexist with the 6-carbon rings at the GB. Even some sp^3 hybridized carbon structures could occur in the highly corrugated GBs. These new structures, like the edge structure of graphene nanoribbon, will open a gap in the Dirac cone at around the Fermi level. The width of the gap will vary at different types of GBs, which means the electron transport property can be significantly affected across the GBs, and the anisotropic transport property may be utilized in a graphene electronic device.

3.4. Grain boundary wrinkles formation mechanism

The asymmetric strain induced corrugations are common structural features inevitably existing at the GB of polycrystalline graphene supported on various substrates. Based on the experimental observations of GB corrugation on both vdW and metallic substrates, it can be concluded that there are two key factors that influence the GB corrugation types and morphological properties. The first one is the neighboring grains misorientation angle, as schematically illustrated in perspective and top-view in Fig. 4(a and b), which determines the intralayer strain distribution at the GB. The second one is the substrate interaction, as demonstrated in the cross-sectional models in Fig. 4(c and d), which provides an essential interlayer influence on the strain distribution at the GB. For the vdW substrate, the morphology of GB corrugations is dominantly affected by the misorientation angle since the substrate

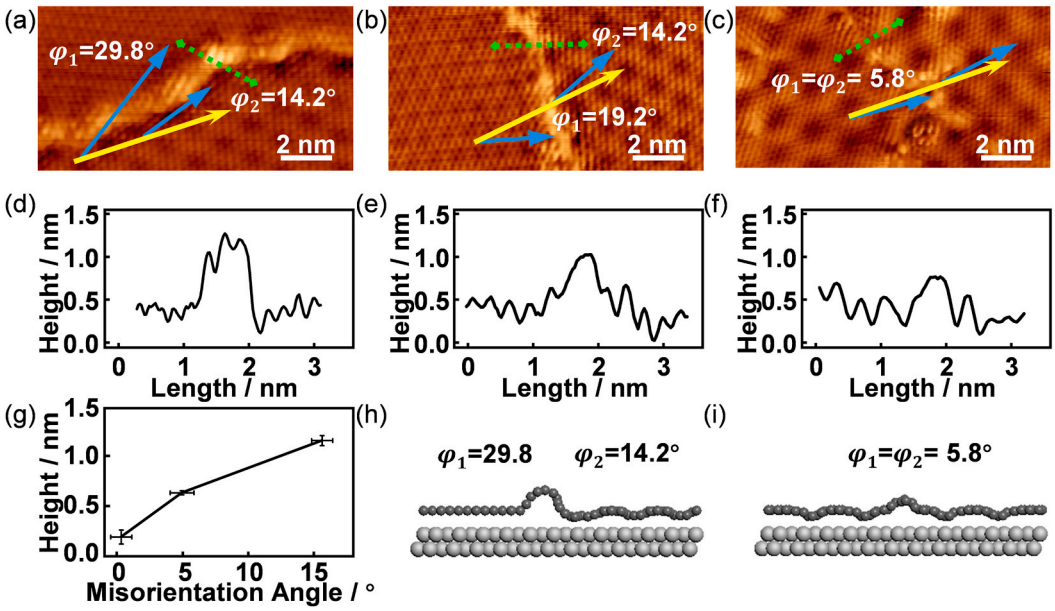

Fig. 3. GB wrinkles on Pt. (a–c) Atomic resolution STM images of three different graphene GB wrinkles on Pt (111) substrate. φ_1 and φ_2 are the twist angles of each grain with respect to the Pt substrate. The zigzag directions of graphene lattices are indicated by the blue arrows (Pt (111) direction indicated by yellow arrows). Angular error $\leq 0.5°$. (d–f) The height measurement along the green dashed arrows in (a–c). (g) Apparent height of GB wrinkles as a function of the misorientation angle $\varphi_1 - \varphi_2$. The error bars indicate a measurement uncertainty of less than 0.9° in angle and of less than 0.07 nm in height. (h, i) The two simple models correspond to monolayer graphene on both sides of the GB having different and the same rotation angles from the Pt(111) substrate, respectively. Dark grey and light grey balls represent C and Pt atoms, respectively. (For interpretation of the references to colour in this figure legend, the reader is referred to the Web version of this article.)

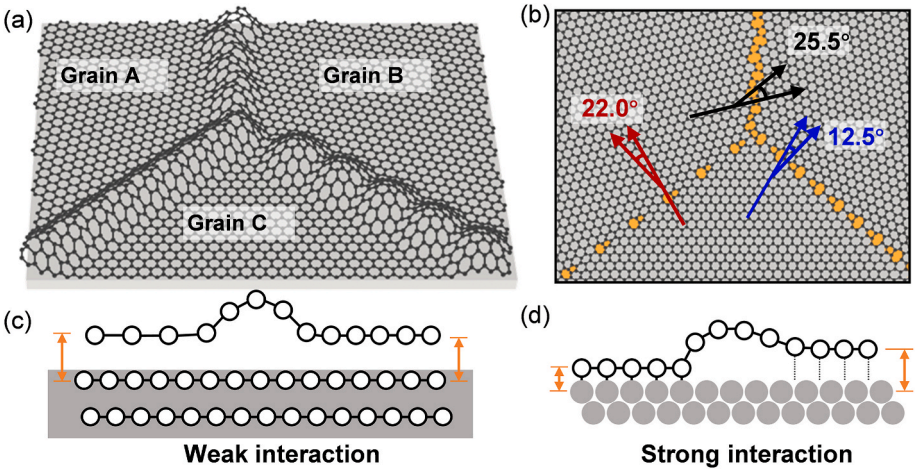

Fig. 4. Illustrations of graphene GB corrugations. (a) Structural model of epitaxial graphene grown on different substrates (HOPG, SiC, or Transition Metal) that exhibit three grains with different lattice orientations. Buckled GB corrugations (between grain A and B, grain A and C, and grain B and C) are shown in a three-dimensional view. (b) Top view of the structural model shows GB corrugations between two grains with misorientation angles of 25.5°, 22.0°, and 12.5°. The zigzag directions of graphene lattices are indicated by the black, red, and blue arrows, respectively. Non-hexagons of GB wrinkles are tagged orange. (c–d) Schematic of GB wrinkles on weakly interacting substrates (c) and strongly interacting substrates (d), respectively. The black circles represent C atoms. Black dashed lines show the correspondence between the graphene layer and the underlying substrates. (For interpretation of the references to colour in this figure legend, the reader is referred to the Web version of this article.)

interaction is weak. The diverse GB corrugation morphology, including bubble chain, straight wrinkle, and irregular wrinkles, would be formed with specific disorientation angles, as shown in Fig. 4(a and b). For the metallic substrates, the morphology of GB corrugations is affected by both factors, since the twist-angle-dependent strong substrate interaction would enhance the asymmetric strain distribution across the GB.

The competition of intralayer and interlayer factors gives rise to a few distinctive morphological features of GB corrugation on vdW and metallic substrates. The cross-sectional profile of the wrinkles on the vdW substrate is generally symmetric. The graphene layer with GB wrinkles is weakly attached to the underlying vdW substrate. Particularly, the GB interaction exceeded the interfacial vdW interaction, facilitating a symmetric medium height wrinkle or bubble chains, as shown in Fig. 4(c). And the bubble could be easily manipulated to switch the polarity.

In contrast, the graphene-metal interaction is much stronger and depends on the registry of C atoms relative to the underlying metal lattice [44]. Highly asymmetric strain might occur at the GB of graphene grains with different registry to the substrate. At the edge of the moiré domain, the carbon atom could be firmly pinned to the substrate since

they are sitting on top of the metal surface-layer atoms underneath [45–47], as shown on the right side of the model in Fig. 4(d). On the other side of the GB, the carbon atoms maintain a large distance to the substrate since they are sitting at the hollow site, as shown on the right side of the model in Fig. 4(d). Such a boundary would result in asymmetric wrinkles, which could not be manipulated to switch the polarity. Additionally, we also recognize that quantitatively addressing of the asymmetric strain distribution mechanism using molecular dynamics (MD) and finite element simulations is important for establishing a universal model, which we will pursue in future works.

4. Conclusion

In conclusion, based on the experimental investigation of the GB corrugation structures of polycrystalline graphene on vdW and metallic substrates, the key factors influencing the morphology and manipulation have been discovered. An asymmetric strain distribution mechanism was proposed to explain the influence of these key factors, i.e., misorientation angle and the graphene-substrate interaction, on the GB corrugations. Specifically, due to the weak interaction with the substrate, GB corrugation with a symmetric profile appears on vdW substrates. They have varying morphologies, i.e., periodic bubble chain, straight wrinkles, and dislocation line, depending on the misorientation angle between neighboring grains. On the other hand, when the interaction with the substrate is strong, as in the case of graphene on Pt(111), both factors contribute to the GB corrugation, which could show a highly asymmetric cross-sectional profile. Notably, symmetric GB wrinkles, also referred to as anti-phase GB, can still form on Pt(111) when the stacking configurations on both sides of the boundary are identical. These findings suggest that asymmetric GB wrinkles are more likely to develop on strongly interacting substrates, whereas symmetric boundaries only exist under specific conditions. Interestingly, we have found that the polarity of the GB bubbles could be reversibly manipulated by using the STM tip with an appropriate tunneling condition. Specifically, the up-downward flipping and right-left switching of GB bubbles can be achieved without breaking any covalent bonds. Our findings would shine light on high precision local strain engineering of polycrystalline graphene as well as other 2D materials.

CRediT authorship contribution statement

Xueyan Li: Writing – review & editing, Writing – original draft, Visualization, Validation, Methodology, Formal analysis, Data curation. **Jiaqi Yang:** Writing – original draft, Software, Investigation, Formal analysis, Data curation. **Yuang Li:** Validation, Methodology, Investigation, Data curation. **Yi Pan:** Writing – review & editing, Writing – original draft, Validation, Supervision, Project administration, Funding acquisition, Conceptualization.

Declaration of competing interest

The authors declare that they have no known competing financial interests or personal relationships that could have appeared to influence the work reported in this paper.

Acknowledgments

This work was financially supported by the National Key Research and Development Program of China (Grant no. 2022YFA1204100) and the National Natural Science Foundation of China (Grant no. 12074302). We thank the Instrument Analysis Center of Xi'an Jiaotong University for the assistance with the measurements.

Appendix A. Supplementary data

Supplementary data to this article can be found online at https://doi.org/10.1016/j.carbon.2025.120890.

References

[1] N. Levy, S.A. Burke, K.L. Meaker, M. Panlasigui, A. Zettl, F. Guinea, et al., Strain-induced pseudo–magnetic fields greater than 300 Tesla in graphene nanobubbles, Science 329 (5991) (2010) 544–547, https://doi.org/10.1126/science.1191700.
[2] O.J. Wahab, E. Daviddi, B. Xin, P.Z. Sun, E. Griffin, A.W. Colburn, et al., Proton transport through nanoscale corrugations in two-dimensional crystals, Nature 620 (7975) (2023) 782–786, https://doi.org/10.1038/s41586-023-06247-6.
[3] H.K. Ng, D. Xiang, A. Suwardi, G. Hu, K. Yang, Y. Zhao, et al., Improving carrier mobility in two-dimensional semiconductors with rippled materials, Nat. Electron. 5 (8) (2022) 489–496, https://doi.org/10.1038/s41928-022-00777-z.
[4] T.P. Darlington, C. Carmesin, M. Florian, E. Yanev, O. Ajayi, J. Ardelean, et al., Imaging strain-localized excitons in nanoscale bubbles of monolayer WSe2 at room temperature, Nat. Nanotechnol. 15 (10) (2020) 854–860, https://doi.org/10.1038/s41565-020-0730-5.
[5] W. Ming, B. Huang, S. Zheng, Y. Bai, J. Wang, J. Wang, et al., Flexoelectric engineering of van der Waals ferroelectric CuInP2S6, Sci. Adv. 8 (33) (2022) eabq1232, https://doi.org/10.1126/sciadv.abq1232.
[6] P. Jia, W. Chen, J. Qiao, M. Zhang, X. Zheng, Z. Xue, et al., Programmable graphene nanobubbles with three-fold symmetric pseudo-magnetic fields, Nat. Commun. 10 (1) (2019) 3127, https://doi.org/10.1038/s41467-019-11038-7.
[7] P. Tonndorf, R. Schmidt, R. Schneider, J. Kern, M. Buscema, G.A. Steele, et al., Single-photon emission from localized excitons in an atomically thin semiconductor, Optica 2 (4) (2015) 347–352, https://doi.org/10.1364/OPTICA.2.000347.
[8] M.M.M. Alyobi, C.J. Barnett, P. Rees, R.J. Cobley, Modifying the electrical properties of graphene by reversible point-ripple formation, Carbon 143 (2019) 762–768, https://doi.org/10.1016/j.carbon.2018.11.076.
[9] X. Huang, W. Zhao, C. Zhu, X. Chen, X. Han, J. Xing, et al., Modification of the interlayer coupling and chemical reactivity of multilayer graphene through wrinkle engineering, Chem. Mater. 33 (7) (2021) 2506–2515, https://doi.org/10.1021/acs.chemmater.0c04799.
[10] R. Zhang, Y. Lai, W. Chen, C. Teng, Y. Sun, L. Yang, et al., Carrier trapping in wrinkled 2D monolayer MoS2 for ultrathin memory, ACS Nano 16 (4) (2022) 6309–6316, https://doi.org/10.1021/acsnano.2c00350.
[11] J. Zhou, X. Long, J. Huang, C. Jiang, F. Zhuo, C. Guo, et al., Multiscale and hierarchical wrinkle enhanced graphene/Ecoflex sensors integrated with human-machine interfaces and cloud-platform, npj Flex. Electron. 6 (1) (2022) 55, https://doi.org/10.1038/s41528-022-00189-1.
[12] P.-Y. Chen, J. Sodhi, Y. Qiu, T.M. Valentin, R.S. Steinberg, Z. Wang, et al., Multiscale graphene topographies programmed by sequential mechanical deformation, Adv. Mater. 28 (18) (2016) 3564–3571, https://doi.org/10.1002/adma.201506194.
[13] U. Manna, M.C.D. Carter, D.M. Lynn, "Shrink-to-Fit" superhydrophobicity: thermally-induced microscale wrinkling of thin hydrophobic multilayers fabricated on flexible shrink-wrap substrates, Adv. Mater. 25 (22) (2013) 3085–3089, https://doi.org/10.1002/adma.201300341.
[14] A.T. N'Diaye, R.v. Gastel, A.J. Martínez-Galera, J. Coraux, H. Hattab, D. Wall, et al., In situ observation of stress relaxation in epitaxial graphene, New J. Phys. 11 (11) (2009) 113056, https://doi.org/10.1088/1367-2630/11/11/113056.
[15] S. Xie, L. Tu, Y. Han, L. Huang, K. Kang, K.U. Lao, et al., Coherent, atomically thin transition-metal dichalcogenide superlattices with engineered strain, Science 359 (6380) (2018) 1131–1136, https://doi.org/10.1126/science.aao5360.
[16] P. Simonis, C. Goffaux, P.A. Thiry, L.P. Biro, P. Lambin, V. Meunier, STM study of a grain boundary in graphite, Surf. Sci. 511 (1) (2002) 319–322, https://doi.org/10.1016/S0039-6028(02)01511-X.
[17] Y. Tison, J. Lagoute, V. Repain, C. Chacon, Y. Girard, F. Joucken, et al., Grain boundaries in graphene on SiC(0001)substrate, Nano Lett. 14 (11) (2014) 6382–6386, https://doi.org/10.1021/nl502854w.
[18] Y. Ogawa, B. Hu, C.M. Orofeo, M. Tsuji, K.-i. Ikeda, S. Mizuno, et al., Domain structure and boundary in single-layer graphene grown on Cu(111) and Cu(100) films, J. Phys. Chem. Lett. 3 (2) (2012) 219–226, https://doi.org/10.1021/jz2015555.
[19] K. Xu, P. Cao, J.R. Heath, Scanning tunneling microscopy characterization of the electrical properties of wrinkles in exfoliated graphene monolayers, Nano Lett. 9 (12) (2009) 4446–4451, https://doi.org/10.1021/nl902729p.
[20] V.M. Pereira, A.H. Castro Neto, H.Y. Liang, L. Mahadevan, Geometry, mechanics, and electronics of singular structures and wrinkles in graphene, Phys. Rev. Lett. 105 (15) (2010) 156603, https://doi.org/10.1103/PhysRevLett.105.156603.
[21] Y. Wang, Y. Wang, C. Xu, X. Zhang, L. Mei, M. Wang, et al., Domain-boundary independency of Raman spectra for strained graphene at strong interfaces, Carbon 134 (2018) 37–42, https://doi.org/10.1016/j.carbon.2018.03.069.
[22] A. Reserbat-Plantey, D. Kalita, Z. Han, L. Ferlazzo, S. Autier-Laurent, K. Komatsu, et al., Strain superlattices and macroscale suspension of graphene induced by corrugated substrates, Nano Lett. 14 (9) (2014) 5044–5051, https://doi.org/10.1021/nl5016552.
[23] Q. Zhao, R. Frisenda, T. Wang, A. Castellanos-Gomez, InSe: a two-dimensional semiconductor with superior flexibility, Nanoscale 11 (20) (2019) 9845–9850, https://doi.org/10.1039/C9NR02172H.
[24] X. Zou, Y. Liu, B.I. Yakobson, Predicting dislocations and grain boundaries in two-dimensional metal-disulfides from the first principles, Nano Lett. 13 (1) (2013) 253–258, https://doi.org/10.1021/nl3040042.

[25] H.W. Kim, W. Ko, J. Ku, I. Jeon, D. Kim, H. Kwon, et al., Nanoscale control of phonon excitations in graphene, Nat. Commun. 6 (1) (2015) 7528, https://doi.org/10.1038/ncomms8528.
[26] N. Néel, C. Steinke, T.O. Wehling, J. Kröger, Inelastic electron tunneling into graphene nanostructures on a metal surface, Phys. Rev. B 95 (16) (2017) 161410, https://doi.org/10.1103/PhysRevB.95.161410.
[27] C. Riedl, C. Coletti, T. Iwasaki, A.A. Zakharov, U. Starke, Quasi-Free-standing epitaxial graphene on SiC obtained by hydrogen intercalation, Phys. Rev. Lett. 103 (24) (2009) 246804, https://doi.org/10.1103/PhysRevLett.103.246804.
[28] M. Gao, Y. Pan, L. Huang, H. Hu, L.Z. Zhang, H.M. Guo, et al., Epitaxial growth and structural property of graphene on Pt(111), Appl. Phys. Lett. 98 (3) (2011) 033101, https://doi.org/10.1063/1.3543624.
[29] H. Hattab, A.T. N'Diaye, D. Wall, G. Jnawali, J. Coraux, C. Busse, et al., Growth temperature dependent graphene alignment on Ir(111), Appl. Phys. Lett. 98 (14) (2011) 141903, https://doi.org/10.1063/1.3548546.
[30] E. Cockayne, G.M. Rutter, N.P. Guisinger, J.N. Crain, P.N. First, J.A. Stroscio, Grain boundary loops in graphene, Phys. Rev. B 83 (19) (2011) 195425, https://doi.org/10.1103/PhysRevB.83.195425.
[31] I. Nikiforov, E. Dontsova, R.D. James, T. Dumitrică, Tight-binding theory of graphene bending, Phys. Rev. B 89 (15) (2014) 155437, https://doi.org/10.1103/PhysRevB.89.155437.
[32] J.M. Carlsson, L.M. Ghiringhelli, A. Fasolino, Theory and hierarchical calculations of the structure and energetics of [0001] tilt grain boundaries in graphene, Phys. Rev. B 84 (16) (2011) 165423, https://doi.org/10.1103/PhysRevB.84.165423.
[33] Z. Tong, A. Pecchia, C. Yam, T. Dumitrica, T. Frauenheim, Phononic thermal transport along graphene grain boundaries: a hidden vulnerability, Adv. Sci. 8 (18) (2021) 2101624, https://doi.org/10.1002/advs.202101624.
[34] K. Kim, Z. Lee, W. Regan, C. Kisielowski, M.F. Crommie, A. Zettl, Grain boundary mapping in polycrystalline graphene, ACS Nano 5 (3) (2011) 2142–2146, https://doi.org/10.1021/nn1033423.
[35] E. Annevelink, B. Xu, H.T. Johnson, E. Ertekin, Shear-coupling of graphene grain boundaries: elementary mechanisms, effects of topology, and role of buckling, Acta. Mater. 244 (2023) 118488, https://doi.org/10.1016/j.actamat.2022.118488.
[36] J. Han, S. Ryu, D. Sohn, S. Im, Mechanical strength characteristics of asymmetric tilt grain boundaries in graphene, Carbon 68 (2014) 250–257, https://doi.org/10.1016/j.carbon.2013.10.085.
[37] T.-H. Liu, G. Gajewski, C.-W. Pao, C.-C. Chang, Structure, energy, and structural transformations of graphene grain boundaries from atomistic simulations, Carbon 49 (7) (2011) 2306–2317, https://doi.org/10.1016/j.carbon.2011.01.063.
[38] J. Zhang, J. Zhao, Structures and electronic properties of symmetric and nonsymmetric graphene grain boundaries, Carbon 55 (2013) 151–159, https://doi.org/10.1016/j.carbon.2012.12.021.
[39] C.-W. Pao, T.-H. Liu, C.-C. Chang, D.J. Srolovitz, Graphene defect polarity dynamics, Carbon 50 (8) (2012) 2870–2876, https://doi.org/10.1016/j.carbon.2012.02.055.
[40] S.A. Iyengar, J.G. McHugh, J.P. Salvage, R. Vajtai, A. Dalton, M. Tripathi, et al., Sub-nm curvature unlocks exceptional inherent flexoelectricity in graphene, arXiv preprint (2025) arXiv: 2503.21996v2.
[41] T. Mashoff, M. Pratzer, V. Geringer, T.J. Echtermeyer, M.C. Lemme, M. Liebmann, et al., Bistability and oscillatory motion of natural nanomembranes appearing within monolayer graphene on silicon dioxide, Nano Lett. 10 (2) (2010) 461–465, https://doi.org/10.1021/nl903133w.
[42] P. Xu, Y. Yang, S.D. Barber, M.L. Ackerman, J.K. Schoelz, D. Qi, et al., Atomic control of strain in freestanding graphene, Phys. Rev. B 85 (12) (2012) 121406, https://doi.org/10.1103/PhysRevB.85.121406.
[43] R. Breitwieser, Y.-C. Hu, Y.C. Chao, R.-J. Li, Y.R. Tzeng, L.-J. Li, et al., Flipping nanoscale ripples of free-standing graphene using a scanning tunneling microscope tip, Carbon 77 (2014) 236–243, https://doi.org/10.1016/j.carbon.2014.05.026.
[44] J. Wintterlin, M.L. Bocquet, Graphene on metal surfaces, Surf. Sci. 603 (10) (2009) 1841–1852, https://doi.org/10.1016/j.susc.2008.08.037.
[45] J. Lahiri, Y. Lin, P. Bozkurt, I.I. Oleynik, M. Batzill, An extended defect in graphene as a metallic wire, Nat. Nanotechnol. 5 (5) (2010) 326–329, https://doi.org/10.1038/nnano.2010.53.
[46] Y. Pan, H. Zhang, D. Shi, J. Sun, S. Du, F. Liu, et al., Highly ordered, millimeter-scale, continuous, single-crystalline graphene monolayer formed on Ru (0001), Adv. Mater. 21 (27) (2009) 2777–2780, https://doi.org/10.1002/adma.200800761.
[47] P.J. Feibelman, Pinning of graphene to Ir(111) by flat Ir dots, Phys. Rev. B 77 (16) (2008) 165419, https://doi.org/10.1103/PhysRevB.77.165419.